

Article

Polymeric Composite including Magnetite Nanoparticles for Hydrogen Peroxide Detection

Maria Roniele Felix Oliveira¹, Pilar Herrasti^{2,*}, Roselayne Ferro Furtado³ , Airis Maria Araújo Melo¹ and Carlucio Roberto Alves¹ 

¹ Department of Chemistry, State University of Ceara, Av. Dr. Silas Munguba 1700, Fortaleza 60740-903, Brazil; roniele.felix@aluno.uece.br (M.R.F.O.); airis.melo@ifpi.edu.br (A.M.A.M.); carlucio.alves@uece.br (C.R.A.)

² Department of Applied Physical Chemistry, Universidad Autónoma de Madrid, Cantoblanco, 28049 Madrid, Spain

³ Embrapa Tropical Agroindustry, Rua Dra. Sara Mesquita 2270, Fortaleza 60511-110, Brazil; roselayne.furtado@embrapa.br

* Correspondence: pilar.herrasti@uam.es

Abstract: The combination of a biopolymer and a conductive polymer can produce new materials with improved physico-chemical and morphological properties that enhance their use as sensors. Magnetite nanoparticles (MN) can be further introduced to these new matrices to improve the analytical performance. This study aimed to evaluate the electrocatalytic response of nanocomposites formed by the introduction of MN to polypyrrole (PPy) doped in the presence of cashew gum polysaccharide (CGP) and in the presence of carboxymethylated cashew gum polysaccharide (CCGP). Characterization of the nanocomposites was carried out via transmission electron microscopy (TEM) and infrared spectroscopy (FTIR) and showed that the absorption band of the blend was shifted to a higher frequency in the nanocomposites, indicating the intermolecular interaction between the blend and nanoparticles. The electrocatalytic performance of the nanocomposites was evaluated by applying a constant potential of -0.7 V with successive additions of H_2O_2 (1 mmol L^{-1}) in 10 mmol L^{-1} phosphate buffer under agitation at pH 7.5. The nanocomposite formed by the introduction of MN to polypyrrole doped with cashew gum polysaccharide (PPy(cgp)-MN) displayed excellent electrocatalytic surface properties, with high H_2O_2 specificity, a linear response ($R^2 = 0.99$), high sensitivity ($0.28 \mu\text{mol L}^{-1}$), and a low H_2O_2 detection limit ($0.072 \text{ mmol L}^{-1}$).

Keywords: hydrogen peroxide; amperometric sensor; cashew gum doping; polypyrrole; magnetite nanoparticles



Citation: Oliveira, M.R.F.; Herrasti, P.; Furtado, R.F.; Melo, A.M.A.; Alves, C.R. Polymeric Composite including Magnetite Nanoparticles for Hydrogen Peroxide Detection. *Chemosensors* **2023**, *11*, 323. <https://doi.org/10.3390/chemosensors11060323>

Academic Editors: Pedro Salazar and Soledad Carinelli

Received: 4 May 2023

Revised: 18 May 2023

Accepted: 21 May 2023

Published: 1 June 2023



Copyright: © 2023 by the authors. Licensee MDPI, Basel, Switzerland. This article is an open access article distributed under the terms and conditions of the Creative Commons Attribution (CC BY) license (<https://creativecommons.org/licenses/by/4.0/>).

1. Introduction

Hydrogen peroxide (H_2O_2) is widely used as an additive in products and processes in the food, personal care, pharmaceutical, and agricultural industries [1]. In the food industry, for example, H_2O_2 is used for the preservation of raw milk due to its antiseptic property [2–5]. However, excessive use of this chemical additive is discouraged because it can cause gastrointestinal problems [6], oxidation of vitamins (such as ascorbic and folic acid) [7], and toxic responses at high concentrations in cells [8]. There is growing interest in the development of effective techniques for the rapid determination of trace H_2O_2 in milk [1,3,4,6,9,10]. In particular, it is important to develop new technologies involving alternative methods of rapid detection in a variety of matrices to produce methods with good sensitivity, a low detection limit, easy reproducibility, and a low cost.

Traditional methods for the detection of H_2O_2 , such as spectrophotometric techniques [11–13], are often laborious and time-consuming. In contrast, an electrochemical method using an amperometric biosensor with immobilized horseradish peroxidase enzyme (HRP) appears to be an effective alternative method [14]. However, the high cost of

the enzyme and the challenge of maintaining its biological activity after immobilization are impediments [15]. Thus, nonenzymatic sensors have been studied in recent years [16–23].

In particular, nonenzymatic sensors based on modified electrodes with nanodimensioned conductive polymers, such as nanostructured polypyrrole (PPy), are considered potential candidates in the development of chemical and electrochemical sensors for the detection of hydrogen peroxide due to their good electrocatalytic response to the detection of H_2O_2 and several advantages attributed to them, such as simplicity and diversity of preparation methods, good electrical conductivity, mechanical resistance, selectivity, and chemical stability [24–28].

Desirable electronic and mechanical characteristics in PPy films can be enhanced by the addition of doping agents by increasing the efficiency of charge transfer by overloading the π bonding orbital along the polymeric chain [29–32]. Cashew gum polysaccharide (CGP) is a heteropolysaccharide that can be used as a polyelectrolyte in aqueous media, with a potential application as a doping agent for the development of polymeric films [32]. Cashew gum polysaccharide (CGP) is an exudate of *Annacardium occidentale*, a natural heteropolysaccharide that meets the requirements of biocompatibility and biodegradability for biomedical/analytical applications [33–35]. As CGP is dissolved in aqueous solution, it becomes a polyelectrolyte, which can be functionalized with appropriate molecules from biological or chemical sources [32,36].

The incorporation of active redox nanoparticles in PPy films, such as magnetic iron nanoparticles (MN), positively affects the analytical performance when they are used as electrochemical signal transducers [29,37]. The presence of MN increases the stability of the film since MN generates a protective effect on the film, causing the preservation of the polaron state [38,39]. Thus, biopolymers with nanoparticles can form nanocomposites that show enhanced electrochemical performance and serve as viable options for the development of novel sensors.

In view of the above considerations, we have developed a novel technique for the electrochemical monitoring of H_2O_2 using a glassy carbon electrode modified by the deposition of nanocomposites formed by magnetite nanoparticles incorporated into combinations of (PPy) and CGP (PPy(cgp)) or carboxymethylated CGP (PPy(ccgp)). Through appropriate characterization techniques (TEM and FTIR), the formation of nanocomposites and the molecular interactions between materials were investigated. Chronoamperometric readings conducted in buffered medium revealed that the PPy(cgp)–MN nanocomposite exhibited the best electrocatalytic properties for the detection and quantification of H_2O_2 . The novelty of this sensor is that it is able to detect hydrogen peroxide in milk, a complex food matrix because of the presence of lipids, carbohydrates, complex proteins, antibiotics, etc. The use of hydrogen peroxide is common to mask contamination with batteries, which is why it is so important to detect this analyte because, in high concentrations (300–800 ppm), it can produce the destruction of lactoperoxidase, an enzyme that prevents the development of bacteria.

2. Materials and Methods

2.1. Reagents

All chemicals used in this study were of analytical grade and used without further purification. Deionized water was processed in Millipore's Milli-Q system (18.2 M Ω cm, at 25 °C). The reagents sulfuric acid (H_2SO_4), ethanol ($\text{CH}_3\text{CH}_2\text{OH}$), potassium ferricyanide ($\text{K}_3[\text{Fe}(\text{CN})_6]$), sodium chloride (NaCl), potassium chloride (KCl), dibasic sodium phosphate dihydrate ($\text{Na}_2\text{HPO}_4 \cdot 2\text{H}_2\text{O}$), potassium phosphate monobasic (KH_2PO_4), NAFION[®] 117 solution, and hydrogen peroxide (H_2O_2 , 30%) were purchased from Sigma-Aldrich (St Louis, MO, USA). Other reagents used were iron (III) chloride hexahydrate ($\text{FeCl}_3 \cdot 6\text{H}_2\text{O}$) (Riedel-de Haën, Offenbach, Germany, 99%), sodium hydroxide (NaOH) (Panreac, San Fernando de Henares, Spain, 98%), methanol (Panreac, 99.9%), and isopropyl alcohol (Riedel-de Haën, $\geq 99.8\%$). The pyrrole monomer (98%, Sigma-Aldrich) was vacuum distilled (59 °C, 50 mmHg) and then protected from light in a dark bottle under refrigeration.

2.2. Isolation and Purification of Polysaccharides

Raw cashew gum was collected from the tree trunk of *Anacardium occidentale* L. cultivated in the experimental field of Embrapa Tropical Agroindustry (coordinates: 4°11'26.62'' S and 38°29'50.78'' W). Isolation and subsequent purification were performed according to the procedure reported by Torquato et al. [40], with adaptations. The gum was milled, dissolved in distilled water at a concentration of 30% (g L⁻¹), and kept at room temperature (25 °C) for 24 h. Afterward, it was centrifuged for 10 min. at 10,000 rpm at 25 °C (to remove tree bark fragments) and precipitated with commercial ethanol (96%) at a ratio of 1:3 (v/v). The precipitated cashew gum polysaccharide (CGP) was filtered, washed with ethanol, and dried in an oven at 60 °C for 24 h. Finally, the extracted CGP was milled to a fine powder, vacuum packed, and kept at room temperature.

2.3. Carboxymethylation of Cashew Gum Polysaccharide

The isolated and purified CGP was subjected to the carboxymethylation reaction according to the methodology reported by Melo et al. and Silva et al. [36,41]. A mixture containing 5 g of CGP was mixed with 5 mL of deionized water until completely homogenized. We then added 10 mol L⁻¹ NaOH (6.2 mL) to the homogeneous solution and stirred for 10 min. The reaction was started after the careful addition of monochloroacetic acid (5.25 g). The mixture was heated at 55 °C for 3 h. The mixture containing carboxymethylated cashew gum polysaccharide (CCGP) was neutralized with 1 mol L⁻¹ HCl and purified by dialysis against deionized water until the elimination of starting reagents or added salt (monitored for water conductivity). The CCGP was subjected to the lyophilization process and stored in vacuum-sealed packages.

2.4. Electrochemical Synthesis of Magnetite Nanoparticles (MN)

Magnetite nanoparticles Fe₃O₄ were synthesized using a flow cell with parallel electrodes according to the procedure developed by Lozano et al. [42]. Eight low-carbon steel sheets (100 mm × 45 mm) of 1 mm thickness and 99.8% pure iron were used as electrodes. The polished electrodes were immersed in 0.04 mol L⁻¹ NaCl. A peristaltic pump operating at 30 rpm with a flow rate of 50 mL min⁻¹ was used, and the total cell volume was 460 mL. A direct current of 700 mA was supplied to the parallel monopolar electrodes. The pH value was measured in the outflow cell. The nanoparticles were collected by the magnetic precipitation method using a neodymium magnet placed at the cell bottom. The supernatant was discarded. The nanoparticles were washed several times with distilled water, collected with a magnet, and then centrifuged at 9000 rpm for 15 min. at room temperature. Drying was carried out in a vacuum system for a period of 24 h.

2.5. Synthesis of Nanocomposites

The nanocomposites were synthesized based on the study developed by Ayad et al. [43] with some adaptations. The chemical polymerization of pyrrole (Py) occurred with either CGP or CCGP in aqueous reaction media and iron oxide nanoparticles (MN) as the oxidizing agent. For each synthesis, solutions of the polysaccharide (1 w/v) were prepared by dissolving 0.5 g in 50 mL of deionized H₂O. In all cases, 0.25 mL of predistilled pyrrole was added, and the resulting solutions were kept for 45 min. under magnetic stirring. Then, 1.41 g of MN was added to the aqueous solutions of each polysaccharide in an ice bath to obtain the respective products PPy_(cgp)-MN and PPy_(ccgp)-MN. The mixtures were stirred overnight, and NaOH solution (50 mL, 0.1 mol L⁻¹) was slowly added to the mixtures. The polymeric nanocomposite (PN) from each synthesis was washed five times with deionized water in an ultrasonic bath for 3 min. and recovered by centrifugation at 9000 rpm/15 min. The last wash was performed with methanol and collected by centrifugation at 9000 rpm/15 min. The PN was finally vacuum dried for 40 h.

2.6. Instrumentation and Characterization

The morphologies of the nanocomposites were studied by transmission electron microscopy (TEM) and Fourier transform infrared spectroscopy (FTIR). For TEM, a single drop (10 μL) of the alcoholic solution containing the PN was placed on a copper grid coated with a carbon film. Photomicrographs were obtained using a JEM 1010 microscope (JEOL, Tokyo, Japan) operating at an acceleration voltage of 100 kV. FTIR was employed to confirm the incorporation of MN in the different matrices using an IFS66v instrument (Bruker, Karlsruhe, Germany).

2.7. Electrochemical Measurements

Measurements involving voltammetric and chronoamperometric techniques were recorded on an Autolab PGSTAT302N potentiostat/galvanostat (Metrohm AG, Herisau, Switzerland) controlled by Nova 11.1 software. A glass cell of 10 mL and a conventional system with three electrodes were adopted, using a vitreous carbon electrode (VC) ($\Phi = 2.7$ mm) as the substrate for the deposition of the different nanocomposites as working electrodes (WE), an Ag/AgCl electrode (3.0 mol L⁻¹ KCl) as the reference electrode, and a platinum helical electrode as the auxiliary electrode.

2.8. Preparation and Modification of the Electrocatalytic Surface

According to the methodology developed by Jaime et al. [44] and with modifications, the different nanocomposites that were synthesized were added directly to the vitreous carbon surface using chemical adsorption and carbon paste preparation. The electrode was gently polished in 0.3 and 0.05 μm alumina powder for 10 min. and carefully washed ultrasonically in absolute ethanol and water for 10 min. each. The electrode was then rinsed with deionized water and dried. The electrode was submitted to cyclic scans of anodic and cathodic potentials in 0.5 mol L⁻¹ H₂SO₄ in a potential range of -0.8 to 2 V at 100 mV s⁻¹. The electrode surface and the assembly steps of the sensors were evaluated by voltammetric measurements at 5.0 mmol L⁻¹ K₃[Fe(CN)₆] and 0.10 mol L⁻¹ KCl in a potential range of -0.7 to 0.75 V. To prepare the carbon paste, we used 1 mL of isopropyl alcohol (4:1), 1 mg of vulcan carbon, and 1 mg of the PN synthesized by the method described above, solubilized for 10 min. in an ultrasonic bath. Subsequently, 8 μL of NAFION[®] was added to the mixture and sonicated for an additional 30 min. The working electrode was prepared with 4 μL of the homogenized suspension on the polished and activated VC surface and then dried overnight.

2.9. Analytical Response

A phosphate buffer solution (PBS) (0.10 mol L⁻¹, pH 7.5) was used as a support electrolyte to evaluate the performance of different electrocatalytic surfaces. Sensor performance was tested by applying a constant potential of -0.7 V with successive additions of 1 mmol L⁻¹ H₂O₂ every 60 s in PBS. The procedure was performed in quintuplicate under continuous stirring.

The sensor performance in samples containing hydrogen peroxide was evaluated for the following parameters: specificity/selectivity, linearity, sensitivity, accuracy, precision (repeatability and reproducibility), and detection limit (LD). For this evaluation, the following equations were used: LD = 3SD/slope, linearity = 10SD/slope, and sensitivity = slope/S, where SD (n = 3) and S are the electrode surfaces.

2.10. Milk Analysis

Whole and skimmed ultrahigh-temperature (UHT) milk samples were purchased in local stores. Both kinds of milk were subjected to amperometric readings without previous dilution, and only the whole milk sample was previously centrifuged to remove fat (5000 rpm at 25 °C for 20 min.) before each electrochemical reading. Amperometric curves and subsequent performance parameters were obtained after applying a constant

potential of -0.7 V with successive additions of $1 \text{ mmol L}^{-1} \text{ H}_2\text{O}_2$ every 60 s under agitation conditions.

3. Results and Discussion

3.1. Characterization of Nanocomposites

Magnetic polymer nanocomposites containing Fe_3O_4 were produced after pyrrole polymerization in the presence of CGP isolated and modified as doping agents. The VC surfaces modified by nanocomposites were subjected to electrochemical readings for the determination of hydrogen peroxide in buffered media and in milk samples.

The structural elucidation confirmed by FTIR spectroscopy reveals the effectiveness of the reaction mixture to form the nanocomposite. The different nanocomposites of $\text{PPy}_{(\text{cgp})}$ and $\text{PPy}_{(\text{ccgp})}$ with iron oxide nanoparticles incorporated in the matrix in aqueous medium have similar bands, e.g., at $3700\text{--}3000 \text{ cm}^{-1}$ (typical for O–H stretch), 2924 and 2860 cm^{-1} (corresponding to the symmetrical and asymmetric stretch vibration of CH of carbon sp^3), and 1640 cm^{-1} (OH vibration for the water molecules bound to the polysaccharide) [45,46] (Figure 1). The absorption peaks present at 1420 cm^{-1} and 1380 cm^{-1} are related to the symmetrical angular deformation of CH_2 and CH_3 in polysaccharides [47,48]. The peaks present in the characteristic absorption band between 1200 and 900 cm^{-1} , more specifically at 1160 , 1070 , and 1020 cm^{-1} , in the different samples can be attributed to carbohydrate and different vibrations of COC and cyclic aliphatic secondary alcohol (C–OH) of glycosidic bonds [47,49]. The spectral difference between the two pure polysaccharides, as reported in the literature, and their respective synthesized nanocomposites is observed by the presence of the adsorption band at 579 cm^{-1} derived from the MN incorporated into the conducting polymer matrices, corresponding to the band typical of elongation vibration from the Fe–O bond [47,50]. It is noticeable that the typical peak for Fe–O in Fe_3O_4 in the nanocomposites is displaced to higher wavelengths when compared to the pure oxide spectrum. This strongly implies effective mixing between the blend segment and the metal oxide particles, which leads to effective intermolecular interactions between the metal oxide particles and the organic groups of polysaccharides, such as hydroxyl or amine groups. A possible molecular structure of the nanocomposite is presented in the inset of Figure 2 based on studies of other polysaccharides [33,43,50] and suggests the intermolecular interactions that occur between the metal oxide particles and the organic groups of the CGP, PPy, and MN. This section may be divided by subheadings. It should provide a concise and precise description of the experimental results, their interpretation, and the experimental conclusions that can be drawn.

TEM images revealed the efficiency of incorporating MN in the different conductive polymeric matrices and reinforced the strong intermolecular interaction between functional groups and MN. The incorporation of MN ($30 \pm 8.8 \text{ nm}$) in the matrices of $\text{PPy}_{(\text{cgp})}$ and $\text{PPy}_{(\text{ccgp})}$ can be seen in Figure 2b,c, respectively. It is clearly observed that a polymeric shell is formed around the MN with the formation of nanocomposites and showed an average thickness of $6.9 \pm 1.78 \text{ nm}$ and $5.4 \pm 2.1 \text{ nm}$ for matrices of $\text{PPy}_{(\text{cgp})}$ and $\text{PPy}_{(\text{ccgp})}$ (average obtained by the shell thickness in different areas of the picture), and this same phenomenon does not occur with the MN obtained electrochemically (Figure 2a). This phenomenon proves a stable structural system because the blend segment remains unbroken after successive washes performed in an ultrasonic bath and further reinforces the strong effective molecular interaction between the doped polymer, the polysaccharides, and the inorganic nanoparticles. Both nanocomposites showed a morphology with dispersed spherical particles of sizes $38.05 \pm 11 \text{ nm}$ and $33.3 \pm 5.9 \text{ nm}$ for nanocomposites formed by $\text{PPy}_{(\text{cgp})}\text{--MN}$ and $\text{PPy}_{(\text{ccgp})}\text{--MN}$ in aqueous medium, respectively.

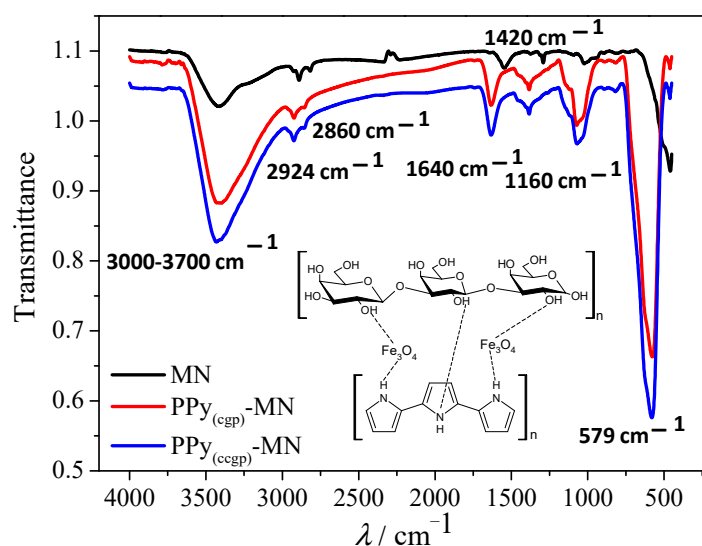


Figure 1. FTIR spectra of different electrocatalytic surfaces synthesized in an aqueous medium in the presence of iron oxide nanoparticles. Inset: structure of the polymeric nanocomposite of $\text{PPy}_{(\text{cgp})}$ -MN.

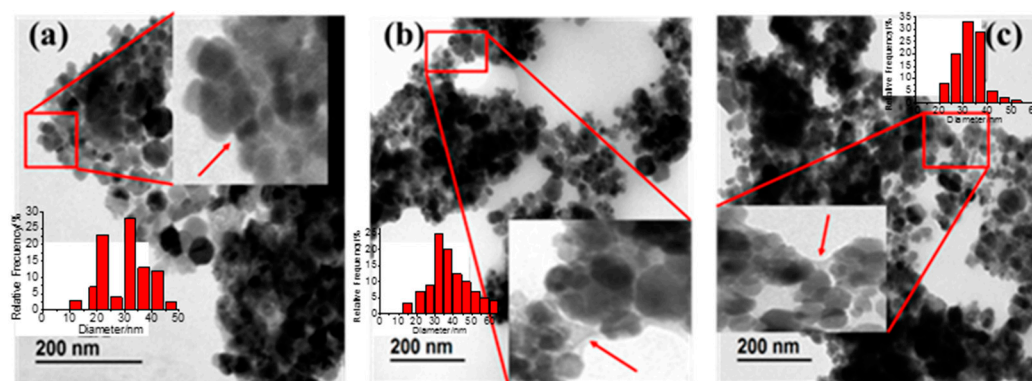


Figure 2. Transmission electron microscopy of the different nanocomposites synthesized. (a) Iron oxide nanoparticle (MN). (b) $\text{PPy}_{(\text{cgp})}$ -MN. (c) $\text{PPy}_{(\text{ccgp})}$ -MN.

3.2. Evaluation of the Analytical Response

Chronoamperometry was used as a technique for electrochemical measurement of the H_2O_2 decomposition process. The choice of the best electrocatalytic surface for this process was made through the modification of the vitreous carbon substrate by chemical adsorption using different nanocomposites formed by $\text{PPy}_{(\text{cgp})}$ and $\text{PPy}_{(\text{ccgp})}$ with nanoparticles in aqueous media.

The amperometric responses showed good performance as H_2O_2 sensors, according to Figure 3. When 1 mmol L^{-1} H_2O_2 was added to pH 7.5 phosphate buffer under conditions controlled by diffusion, an initial increase in peak current was noted, demonstrating effective electrocatalytic reduction of H_2O_2 . Subsequent additions of H_2O_2 at regular intervals resulted in a drastic change in electrical current because the increase in the magnitude of the reduction peak was proportional to the H_2O_2 concentration and steady-state formation.

It was also observed in the chronoamperogram that throughout the reading time and successive additions of H_2O_2 , a slight decline in the reduction current amplitude in the final min. was noted for the two nanocomposites formed by $\text{PPy}_{(\text{cgp})}$ -MN and $\text{PPy}_{(\text{ccgp})}$ -MN. This can be associated with the relationship between the increased H_2O_2 concentration and the possible electrocatalytic surface poisoning by the analyte. At low levels of H_2O_2 , the concentration next to the electrode surface is rapidly depleted as the substrate is converted

to the product by the catalytic action of the nanoparticle, resulting in a high sensitivity of the electrode response [51]. Successive additions of the analyte solution to the same electrochemical system cause an increase in the concentration of H_2O_2 and, consequently, a saturation of the system by the excessive reaction product, thereby bringing about surface poisoning because there will be less deposition of the substrate to act on the catalytic activity of H_2O_2 , and as a result, a lower slope is found [3].

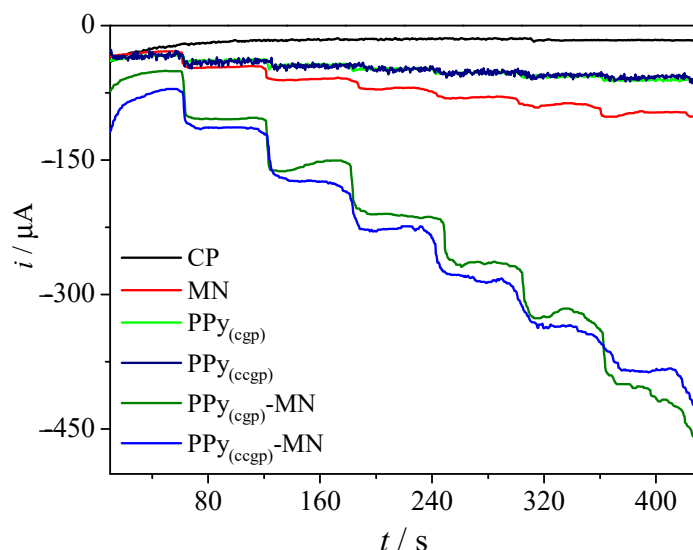


Figure 3. Amperometric responses at -0.7 V in PBS buffer, pH 7.5, from the VC electrode modified by polymeric nanocomposites with additions of 1 mmol L^{-1} H_2O_2 at regular intervals of 60 s. CP—carbon paste; MN—iron magnetite nanoparticles; PPy—polypyrrole; CGP—cashew gum polysaccharide; CCGP—carboxymethylated cashew gum polysaccharide.

The significant improvement in the electrocatalytic performance of the sensors is observed in the nanocomposites that have the greatest reduction current for H_2O_2 , and this improvement can be attributed to the protective effect that the oxide nanoparticles have on the sensor platform with polypyrrole. The H_2O_2 electrons, when penetrating the polymer, reduce the volume fraction of the conductive particles and, therefore, reduce the number of conducting pathways for charge carriers, causing an increase in the electrical resistance of the polymer and, consequently, a decrease in the current crossing the polymer [4,37,52]. MN contributes to the preservation of the state of the polaron in the polypyrrole, and consequently, it will have greater stability and conductivity, positively affecting the sensitivity and detection limit of the H_2O_2 sensor platform [29,38].

Both electrodes modified by nanocomposites $\text{PPy}_{(\text{cgp})}\text{-MN}$ and $\text{PPy}_{(\text{ccgp})}\text{-MN}$ showed good electrochemical responses to H_2O_2 with linearities of 0.996 and 0.994, respectively, and sensitivities of 2.8×10^{-4} and $3.8 \times 10^{-4} \mu\text{AmM}^{-1}$. The chronoamperometric curves of the two nanocomposites showed no significant difference in electrocatalytic activity in relation to hydrogen peroxide at concentrations of 0.1 at 0.9 mmol L^{-1} . Therefore, it was decided to continue only with the $\text{PPy}_{(\text{cgp})}\text{-MN}$ nanocomposite to evaluate the electrocatalytic potential of the sensor platform, as the addition of a carbonyl group in the polysaccharide structure, acting as a doping agent, did not generate a significant improvement in the catalytic activity against H_2O_2 for this application. For these reasons, the performance evaluation study was conducted only on the nanocomposite based on CGP.

The $\text{PPy}_{(\text{cgp})}\text{-MN}$ platform presented a linear increase in current and reached the maximum steady-state current in 2 to 4 s. The sensor curve (Figure 4a) presented a detection limit of $71.6 \mu\text{M}$, estimated by the equation from the standard deviation of the blank and the angular coefficient (slope) of the analytical curve [43]. The linear behavior follows the equation $y = 3.8 \times 10^{-4} x + 6.34 \times 10^{-5}$. The detection limit shown by the $\text{PPy}_{(\text{cgp})}\text{-MN}$ nanocomposite outstrips previous reports on a magnetite sensor by Cao et al.

with a detection limit of 1 mmol L^{-1} [19] and a microfluidic paper-based analytical device by Lima et al. with a detection limit of $3.54 \times 10^{-4} \text{ mol L}^{-1}$ [10]. It is worth noting that the detection limit expressed by the sensor platform developed herein is low enough to satisfy the requirement for the determination of H_2O_2 residues in food [52]

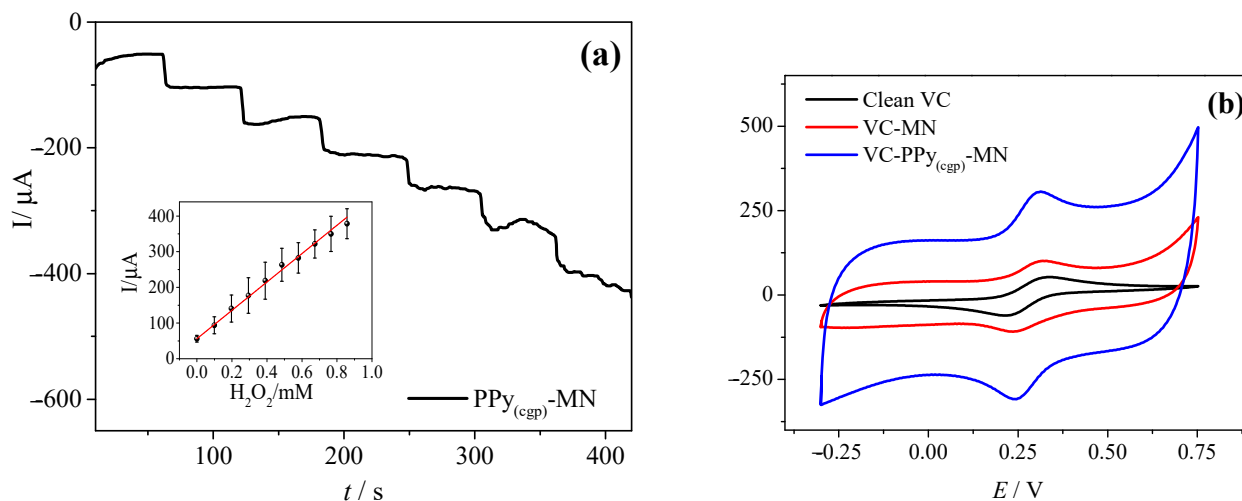


Figure 4. (a) Analytical curve of vitreous carbon electrode modified by $\text{PPy}_{(\text{cgp})}\text{-MN}$ with gradual additions of $1 \text{ mmol L}^{-1} \text{ H}_2\text{O}_2$ every 60 s. The insert is the linear relationship between cathode current magnitude and H_2O_2 concentration in a range from 0.1 to 0.9 M, with a potential of -0.7 V . (b) Cyclic voltammograms of the electroactive surfaces on the vitreous carbon substrate at $5.0 \text{ mmol L}^{-1} \text{ K}_3[\text{Fe}(\text{CN})_6]$ and $0.1 \text{ mol L}^{-1} \text{ KCl}$ at 100 mV s^{-1} . VC—vitreous carbon; MN—magnetite nanoparticles; $\text{PPy}_{(\text{cgp})}\text{-MN}$ —nanocomposite of cashew gum, polypyrrole, and magnetite synthesized in aqueous medium.

By electrochemical characterization of the vitreous carbon surface modified with the magnetite nanocomposite in the presence of an electrolytic solution of $5.0 \text{ mmol L}^{-1} \text{ K}_3[\text{Fe}(\text{CN})_6]$ and $0.1 \text{ mol L}^{-1} \text{ KCl}$, it was possible to further reinforce the efficiency of the process and the effect on the electronic transfer caused by the incorporation of MN into the nanocomposite. The voltammetric profile, shown in Figure 4b, reveals that the presence of MN increases the electron transfer, the ratio between peak currents with only nanoparticles and with the composite increases by a value greater than 2.5 ($I_p(\text{VCPy}_{(\text{cgp})}\text{-MN})/I_p(\text{VC-MN})$), and consequently improves the electrocatalytic properties of the matrix based on cashew gum and polypyrrole ($\text{PPy}_{(\text{cgp})}$). The presence of MN generates an increase in the electrode surface area, which is confirmed by the difference in the increase in electron transfer among the different phases of the electrocatalytic platform development process. For this reason, the amperometric response in relation to H_2O_2 is visibly improved because MN favors a better electrocatalytic reduction of H_2O_2 [1]. With these characteristics, the $\text{PPy}_{(\text{cgp})}\text{-MN}$ nanomaterial is promising for applications in electrochemical devices, such as sensors and capacitors.

The selectivity of the sensors in the presence of interfering species in pH 7.5 phosphate buffer was evaluated in this study (Figure 5). The results indicate no change in the catalytic capacity for ascorbic acid, glucose, urea, ethanol, sodium chloride, and lithium perchlorate at concentrations that were ten times higher than H_2O_2 . These results confirm that the surface modified with the $\text{PPy}_{(\text{cgp})}\text{-MN}$ nanocomposite exhibited excellent electrochemical performance due to the absence of any appreciable interference signal in the electrolyte, thus demonstrating excellent selectivity for the analyte of interest. In parallel to this result, we also justify the choice of a working potential of -0.7 V because this potential does not cause the oxidation of possible interfering substances.

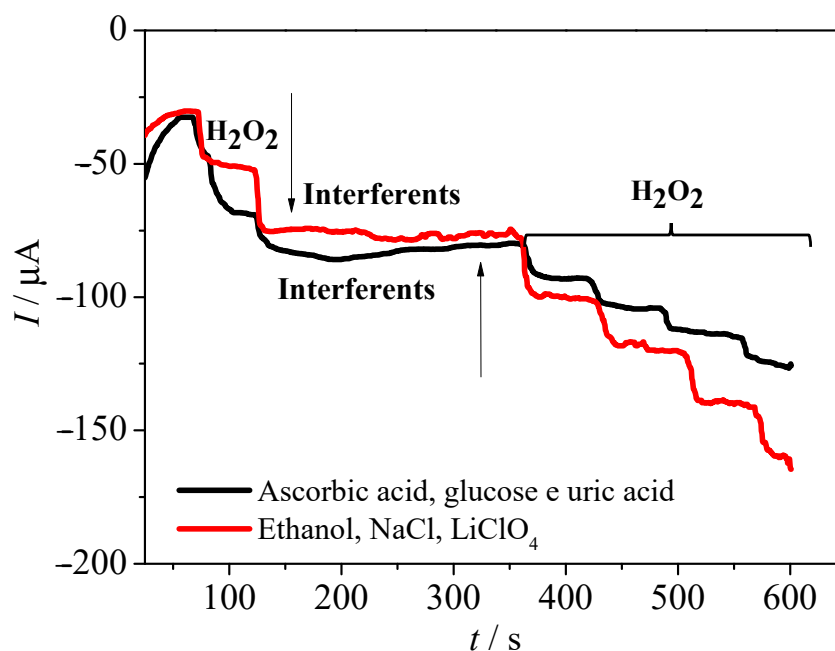


Figure 5. Amperometric response of PPy_(cgp)-MN surface with intermittent additions of H₂O₂ and interfering species every 60 s at -0.7 V in phosphate buffer pH 7.5.

The reproducibility of the modified surface with chemical adsorption of PPy_(cgp)-MN was investigated by the amperometric responses. The electrocatalytic behavior of four successive assemblies was observed, providing a relative standard deviation (RSD) of 4.66% after nine injections of 1 mmol L^{-1} H₂O₂ in PBS buffer per assembly (Figure 6a). Therefore, the reproducibility is acceptable when compared to other studies already reported by Ping et al. [4], where the RSD was less than 4.7%.

The possible reuse of the PPy_(cgp)-MN sensor was evaluated using the same electrode for five successive measurements (Figure 6b) with the addition of 1 mmol L^{-1} H₂O₂ every 60 s. The coefficients of variance (CV) were 1.80%, 0.24%, 0.21%, 0.25%, 0.23%, 0.47%, 0.27%, 2.44%, and 0.27% for the respective concentrations of 0.1, 0.2, 0.3, 0.4, 0.5, 0.6, 0.7, 0.8, and 0.9 mmol L^{-1} H₂O₂. The low CV values indicate that the sensors maintain satisfactory electrochemical stability and that they can be reused for different measurements. The increase in current with the use of the electrode could be due to the conditioning of the electrode when it is used at different times.

The viability of the amperometric sensor proposed for the detection of H₂O₂ in milk samples was obtained through the amperometric curve in current time and constant potential using the CV electrode modified with PPy_(cgp)-MN under optimal conditions (Figure 7). The nanocomposite showed a lower baseline than the PBS readings, which can be attributed to electrode surface fouling in milk samples [4]. The sensor showed sensitivities of 5.6×10^{-5} and $1.7 \times 10^{-4} \text{ } \mu\text{A mM}^{-1}$ and detection limits of 0.53 and 0.13 mmol L^{-1} for skimmed and whole milk, respectively. These data represent satisfactory performance for the determination of H₂O₂ in the two different types of milk because of the rapid response and the significant increase in the reduction current after the consecutive addition of 1 mmol L^{-1} H₂O₂. Thus, the new materials developed from the cashew gum polysaccharide behaved as excellent sensor platforms for the testing of H₂O₂ in foods.

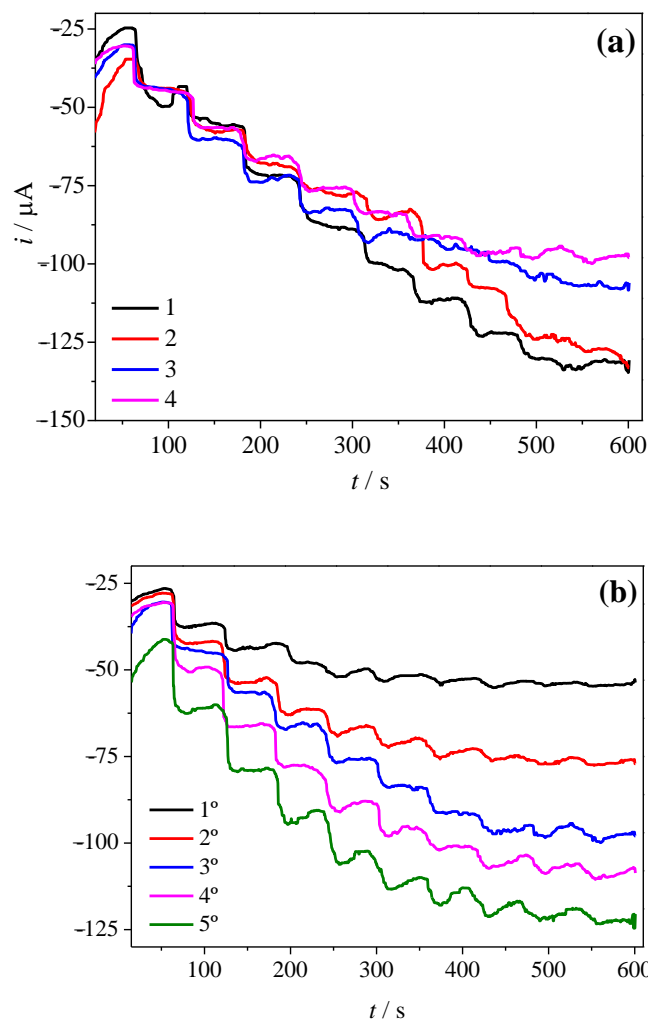


Figure 6. (a) Amperometric responses of different assemblies of $\text{PPy}_{(\text{cgp})}$ -MN sensors at -0.7 V in phosphate buffer at pH 7.5 with successive additions of $1 \text{ mmol L}^{-1} \text{ H}_2\text{O}_2$ at predefined time intervals. (b) Amperometric response of successive use of the same electrode modified with $\text{PPy}_{(\text{cgp})}$ -MN at -0.7 V under the same conditions as (a).

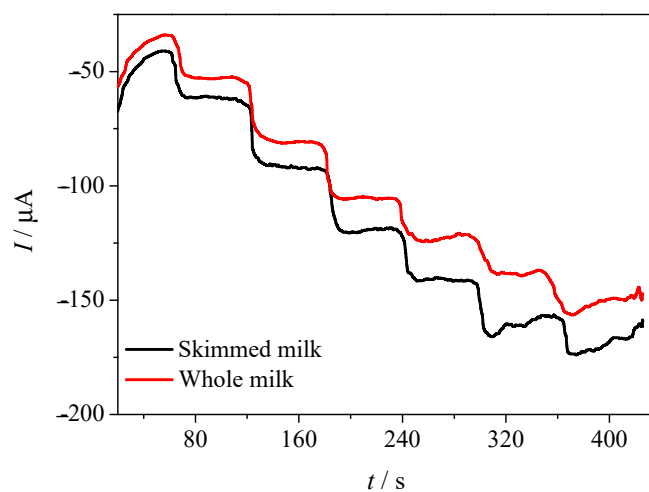


Figure 7. Amperometric response of H_2O_2 determination in whole milk and skimmed UHT using the modified electrode containing $\text{PPy}_{(\text{cgp})}$ -MN.

4. Conclusions

In this work, we designed and fabricated a new nonenzymatic sensor from a $\text{PPy}_{(\text{cgp})}$ -MN nanocomposite. This material provided a better electrocatalytic surface than the other surfaces tested in this study and exhibited good sensitivity and specificity for H_2O_2 detection, including milk contaminated with H_2O_2 . This sensor demonstrated good performance with a low detection limit, good reproducibility, and potential reuse for consecutive measurements.

The fast response and higher reduction current of H_2O_2 by nanocomposite-modified electrodes stand out in relation to other electrocatalytic surfaces. This superior performance for the decomposition of the analyte of interest verified that the presence of Fe_3O_4 nanoparticles in the composition of the electrocatalytic nanomaterial, together with the conductive properties derived from the conductive composite, were effective and contributed favorably to the reduction of H_2O_2 . Thus, our materials are electrochemically more stable and conductive and can increase the surface area of the electrodes.

Furthermore, in this work, we used cashew gum, a renewable natural resource of high availability but relatively low value, to produce the nanocomposite sensor, together with the incorporation of magnetite nanoparticles and polypyrrole. The novel use of cashew gum for this application adds potential economic value to the cashew production chain and is beneficial to cashew gum producers and their countries.

Author Contributions: Conceptualization, C.R.A. and P.H.; methodology, M.R.F.O. and A.M.A.M.; validation, M.R.F.O., C.R.A., P.H. and R.F.F.; formal analysis, C.R.A., P.H. and R.F.F.; investigation, M.R.F.O., P.H. and A.M.A.M.; data curation, M.R.F.O. and P.H.; writing—original draft preparation, M.R.F.O. and A.M.A.M.; writing—review and editing, C.R.A., P.H. and R.F.F.; visualization, C.R.A.; supervision, P.H.; funding acquisition, C.R.A., P.H. and R.F.F. All authors have read and agreed to the published version of the manuscript.

Funding: This research was funded by Spanish Ministry of Science and Innovation, grant number PID2021-123431OB-I00 and the Brazilian agencies, CAPES, FUNCAP and CNPQ, Embrapa Tropical Agroindustry.

Data Availability Statement: Not applicable.

Conflicts of Interest: The authors declare no conflict of interest.

References

1. Karimi, A.; Husain, S.W.; Hosseini, M.; Azar, P.A.; Ganjali, M.R. Rapid and Sensitive Detection of Hydrogen Peroxide in Milk by Enzyme-Free Electrochemiluminescence Sensor Based on a Polypyrrole-Cerium Oxide Nanocomposite. *Sens. Actuators B Chem.* **2018**, *271*, 90–96. [[CrossRef](#)]
2. Brul, S.; Coote, P. Preservative Agents in Foods: Mode of Action and Microbial Resistance Mechanisms. *Int. J. Food Microbiol.* **1999**, *50*, 1–17. [[CrossRef](#)]
3. Dong, X.X.; Li, M.Y.; Feng, N.N.; Sun, Y.M.; Yang, C.; Xu, Z.L. A Nanoporous MgO Based Nonenzymatic Electrochemical Sensor for Rapid Screening of Hydrogen Peroxide in Milk. *RSC Adv.* **2015**, *5*, 86485–86489. [[CrossRef](#)]
4. Ping, J.; Mao, X.; Fan, K.; Li, D.; Ru, S.; Wu, J.; Ying, Y. A Prussian Blue-Based Amperometric Sensor for the Determination of Hydrogen Peroxide Residues in Milk. *Ionics* **2010**, *16*, 523–527. [[CrossRef](#)]
5. Juven, B.J.; Pierson, M.D. Antibacterial Effects of Hydrogen Peroxide and Methods for Its Detection and Quantitation. *J. Food Prot.* **1996**, *59*, 1233–1241. [[CrossRef](#)] [[PubMed](#)]
6. Silva, R.A.B.; Montes, R.H.O.; Richter, E.M.; Munoz, R.A.A. Rapid and Selective Determination of Hydrogen Peroxide Residues in Milk by Batch Injection Analysis with Amperometric Detection. *Food Chem.* **2012**, *133*, 200–204. [[CrossRef](#)]
7. Taher, M.M.; Lakshmaiah, N. Folic Acid Stability in Hydrogen Peroxide-Potassium Thiocyanate-Treated Milk. *Food Chem.* **1992**, *44*, 343–347. [[CrossRef](#)]
8. Wei, Y.; Guo, M. Hydrogen Peroxide Triggered Prochelor Activation, Subsequent Metal Chelation, and Attenuation of the Fenton Reaction. *Angew. Chem. Int. Ed.* **2007**, *46*, 4722–4725. [[CrossRef](#)] [[PubMed](#)]
9. Bollella, P.; Medici, L.; Tessema, M.; Poloznikov, A.A.; Hushpulian, D.M.; Tishkov, V.I.; Andreu, R.; Leech, D.; Megersa, N.; Marcaccio, M.; et al. Highly Sensitive, Stable and Selective Hydrogen Peroxide Amperometric Biosensors Based on Peroxidases from Different Sources Wired by Os-Polymer: A Comparative Study. *Solid State Ion.* **2018**, *314*, 178–186. [[CrossRef](#)]
10. Lima, L.S.; Rossini, E.L.; Pezza, L.; Pezza, H.R. Bioactive Paper Platform for Detection of Hydrogen Peroxide in Milk. *Spectrochim. Acta Part A Mol. Biomol. Spectrosc.* **2020**, *227*, 117774. [[CrossRef](#)]

11. Gubitz, G.; Van Zoonen, P.; Gooijer, C.; Velthorst, N.H.; Frei, R.W. Immobilized Fluorophores in Dynamic Chemiluminescence Detection of Hydrogen Peroxide. *Anal. Chem.* **1985**, *57*, 2071–2074. [[CrossRef](#)]
12. Chen, W.; Li, B.; Xu, C.; Wang, L. Chemiluminescence Flow Biosensor for Hydrogen Peroxide Using DNAzyme Immobilized on Eggshell Membrane as a Thermally Stable Biocatalyst. *Biosens. Bioelectron.* **2009**, *24*, 2534–2540. [[CrossRef](#)]
13. Matsubara, C.; Kawamoto, N.; Takamura, K. Oxo[5, 10, 15, 20-Tetra(4-Pyridyl)Porphyrinato]Titanium(IV): An Ultra-High Sensitivity Spectrophotometric Reagent for Hydrogen Peroxide. *Analyst* **1992**, *117*, 1781–1784. [[CrossRef](#)]
14. Yalçın, F.; Çevik, E.; Şenel, M.; Baykal, A. Development of an Amperometric Hydrogen Peroxide Biosensor Based on the Immobilization of Horseradish Peroxidase onto Nickel Ferrite Nanoparticle-Chitosan Composite. *Nano-Micro Lett.* **2011**, *3*, 91–98. [[CrossRef](#)]
15. Ammam, M. Electrochemical and Electrophoretic Deposition of Enzymes: Principles, Differences and Application in Miniaturized Biosensor and Biofuel Cell Electrodes. *Biosens. Bioelectron.* **2014**, *58*, 121–131. [[CrossRef](#)] [[PubMed](#)]
16. Meier, J.; M Hofferber, E.; A Stapleton, J.; Iverson, N.M. Hydrogen Peroxide Sensors for Biomedical Applications. *Chemosensors* **2019**, *7*, 64. [[CrossRef](#)]
17. Zhao, S.; Danley, M.; Ward, J.E.; Li, D.; Mincer, T.J. An Approach for Extraction, Characterization and Quantitation of Microplastic in Natural Marine Snow Using Raman Microscopy. *Anal. Methods* **2017**, *9*, 1470–1478. [[CrossRef](#)]
18. Prabhu, P.; Babu, R.S.; Narayanan, S.S. Synergetic Effect of Prussian Blue Film with Gold Nanoparticle Graphite–Wax Composite Electrode for the Enzyme-Free Ultrasensitive Hydrogen Peroxide Sensor. *J. Solid State Electrochem.* **2014**, *18*, 883–891. [[CrossRef](#)]
19. Jaime-González, J.; Mazario, E.; Menendez, N.; Sanchez-Marcos, J.; Muñoz-Bonilla, A.; Herrasti, P. Comparison of Ferrite Nanoparticles Obtained Electrochemically for Catalytical Reduction of Hydrogen Peroxide. *J. Solid State Electrochem.* **2016**, *20*, 1191–1198. [[CrossRef](#)]
20. Keerthi, M.; Boopathy, G.; Chen, S.-M.; Chen, T.-W.; Lou, B.-S. A Core-Shell Molybdenum Nanoparticles Entrapped f-MWCNTs Hybrid Nanostructured Material Based Non-Enzymatic Biosensor for Electrochemical Detection of Dopamine Neurotransmitter in Biological Samples. *Sci. Rep.* **2019**, *9*, 13075. [[CrossRef](#)]
21. Cao, G.S.; Wang, P.; Li, X.; Wang, Y.; Wang, G.; Li, J. Hydrogen Peroxide Electrochemical Sensor Based on Fe₃O₄ Nanoparticles. *Micro Nano Lett.* **2014**, *9*, 16–18. [[CrossRef](#)]
22. Manivel, A.; Anandan, S. Silver Nanoparticles Embedded Phosphomolybdate–Polyaniline Hybrid Electrode for Electrocatalytic Reduction of H₂O. *J. Solid State Electrochem.* **2011**, *15*, 153–160. [[CrossRef](#)]
23. Afraz, A.; Rafati, A.A.; Hajian, A. Analytical Sensing of Hydrogen Peroxide on Ag Nanoparticles–Multiwalled Carbon Nanotube-Modified Glassy Carbon Electrode. *J. Solid State Electrochem.* **2013**, *17*, 2017–2025. [[CrossRef](#)]
24. Jin, E.; Bian, X.; Lu, X.; Wang, C. Fabrication of Multiwalled Carbon Nanotubes/Polypyrrole/Prussian Blue Ternary Composite Nanofibers and Their Application for Enzymeless Hydrogen Peroxide Detection. *J. Mater. Sci.* **2012**, *47*, 4326–4331. [[CrossRef](#)]
25. Xing, L.; Rong, Q.; Ma, Z. Non-Enzymatic Electrochemical Sensing of Hydrogen Peroxide Based on Polypyrrole/Platinum Nanocomposites. *Sens. Actuators B Chem.* **2015**, *221*, 242–247. [[CrossRef](#)]
26. Tao, Y.; Ju, E.; Ren, J.; Qu, X. Polypyrrole Nanoparticles as Promising Enzyme Mimics for Sensitive Hydrogen Peroxide Detection. *Chem. Commun.* **2014**, *50*, 3030–3032. [[CrossRef](#)]
27. Zhang, T.; Yuan, R.; Chai, Y.; Li, W.; Ling, S. A Novel Nonenzymatic Hydrogen Peroxide Sensor Based on a Polypyrrole Nanowire-Copper Nanocomposite Modified Gold Electrode. *Sensors* **2008**, *8*, 5141–5152. [[CrossRef](#)]
28. Akhtar, M.A.; Hayat, A.; Iqbal, N.; Marty, J.L.; Nawaz, M.H. Functionalized Graphene Oxide–Polypyrrole–Chitosan (FGO–PPy–CS) Modified Screen-Printed Electrodes for Non-Enzymatic Hydrogen Peroxide Detection. *J. Nanoparticle Res.* **2017**, *19*, 334. [[CrossRef](#)]
29. Montoya, P.; Mejía, S.; Gonçalves, V.R.; De Torresi, S.I.C.; Calderón, J.A. Performance Improvement of Macroporous Polypyrrole Sensor for Detection of Ammonia by Incorporation of Magnetite Nanoparticles. *Sens. Actuators B Chem.* **2015**, *213*, 444–451. [[CrossRef](#)]
30. Ansari, R. Polypyrrole Conducting Electroactive Polymers: Synthesis and Stability Studies. *E-J. Chem.* **2006**, *3*, 860413. [[CrossRef](#)]
31. Duchet, J.; Legras, R.; Demoustier-Champagne, S. Chemical Synthesis of Polypyrrole: Structure–Properties Relationship. *Synth. Met.* **1998**, *98*, 113–122. [[CrossRef](#)]
32. Castro, R.A.O.; Monte, R.S.; Mendes, L.G.; Furtado, R.F.; Silva, Â.R.A.; Biswas, A.; Cheng, H.N.; Alves, C.R. Electrosynthesis and Characterization of Polypyrrole/Cashew Gum Composite Grown on Gold Surface in Aqueous Medium. *Int. J. Electrochem. Sci.* **2017**, *12*, 50–61. [[CrossRef](#)]
33. Ramesan, M.T.; Siji, C.; Kalaprasad, G.; Bahuleyan, B.K.; Al-Maghrabi, M.A. Effect of Silver Doped Zinc Oxide as Nanofiller for the Development of Biopolymer Nanocomposites from Chitin and Cashew Gum. *J. Polym. Environ.* **2018**, *26*, 2983–2991. [[CrossRef](#)]
34. Araújo, I.M.S.; Zampa, M.F.; Moura, J.B.; dos Santos, J.R., Jr.; Eaton, P.; Zucolotto, V.; Veras, L.M.C.; De Paula, R.C.M.; Feitosa, J.P.A.; Leite, J. Contribution of the Cashew Gum (*Anacardium occidentale* L.) for Development of Layer-by-Layer Films with Potential Application in Nanobiomedical Devices. *Mater. Sci. Eng. C* **2012**, *32*, 1588–1593. [[CrossRef](#)] [[PubMed](#)]
35. Eiras, C.; Passos, I.N.G.; de Brito, A.C.F.; dos Santos Júnior, J.R.; Zucolotto, V.; Oliveira, O.N., Jr.; Kitagawa, I.L.; Constantino, C.J.L.; da Cunha, H.N. Nanocompósitos Eletroativos de Poli-o-Metoxianilina e Polissacarídeos Naturais. *Quim. Nova* **2007**, *30*, 1158–1162. [[CrossRef](#)]

36. Silva, D.A.; De Paula, R.C.; Feitosa, J.P.A.; De Brito, A.C.; Maciel, J.S.; Paula, H.C.B. Carboxymethylation of Cashew Tree Exudate Polysaccharide. *Carbohydr. Polym.* **2004**, *58*, 163–171. [[CrossRef](#)]
37. Wu, Y.; Xing, S.; Jing, S.; Zhou, T.; Zhao, C. Examining the Use of Fe₃O₄ Nanoparticles to Enhance the NH₃ Sensitivity of Polypyrrole Films. *Polym. Bull.* **2007**, *59*, 227–234. [[CrossRef](#)]
38. Montoya, P.; Jaramillo, F.; Calderón, J.; Córdoba De Torresi, S.I.; Torresi, R.M. Evidence of Redox Interactions between Polypyrrole and Fe₃O₄ in Polypyrrole-Fe₃O₄ Composite Films. *Electrochim. Acta* **2010**, *55*, 6116–6122. [[CrossRef](#)]
39. Chen, A.; Wang, H.; Li, X. Influence of Concentration of FeCl₃ Solution on Properties of Polypyrrole-Fe₃O₄ Composites Prepared by Common Ion Absorption Effect. *Synth. Met.* **2004**, *145*, 153–157. [[CrossRef](#)]
40. Torquato, D.S.; Ferreira, M.L.; Sá, G.C.; Brito, E.S.; Pinto, G.A.S.; Azevedo, E.H.F. Evaluation of Antimicrobial Activity of Cashew Tree Gum. *World J. Microbiol. Biotechnol.* **2004**, *20*, 505–507. [[CrossRef](#)]
41. Melo, A.M.A.; Oliveira, M.R.F.; Furtado, R.F.; de Fatima Borges, M.; Biswas, A.; Cheng, H.N.; Alves, C.R. Preparation and Characterization of Carboxymethyl Cashew Gum Grafted with Immobilized Antibody for Potential Biosensor Application. *Carbohydr. Polym.* **2020**, *228*, 115408. [[CrossRef](#)]
42. Lozano, I.; López, C.; Menendez, N.; Casillas, N.; Herrasti, P. Design, Construction and Evaluation of a 3D Printed Electrochemical Flow Cell for the Synthesis of Magnetite Nanoparticles. *J. Electrochem. Soc.* **2018**, *165*, H688–H697. [[CrossRef](#)]
43. Ayad, M.; Salahuddin, N.; Fayed, A.; Bastakoti, B.P.; Suzuki, N.; Yamauchi, Y. Chemical Design of a Smart Chitosan–Polypyrrole–Magnetite Nanocomposite toward Efficient Water Treatment. *Phys. Chem. Chem. Phys.* **2014**, *16*, 21812–21819. [[CrossRef](#)]
44. Jaime, J.; Rangel, G.; Muñoz-Bonilla, A.; Mayoral, A.; Herrasti, P. Magnetite as a Platform Material in the Detection of Glucose, Ethanol and Cholesterol. *Sens. Actuators B Chem.* **2017**, *238*, 693–701. [[CrossRef](#)]
45. Srivastava, A.; Tripathy, J.; Mishra, M.M.; Behari, K. Modification of Guar Gum through Grafting of 4-vinyl Pyridine Using Potassium Peroxymonosulphate/Ascorbic Acid Redox Pair. *J. Appl. Polym. Sci.* **2007**, *106*, 1353–1358. [[CrossRef](#)]
46. da Silva Perez, D.; Montanari, S.; Vignon, M.R. TEMPO-Mediated Oxidation of Cellulose III. *Biomacromolecules* **2003**, *4*, 1417–1425. [[CrossRef](#)]
47. Ramesan, M.T.; Surya, K. Synthesis, Characterization, and Properties of Cashew Gum Graft Poly (Acrylamide)/Magnetite Nanocomposites. *J. Appl. Polym. Sci.* **2016**, *133*, 22. [[CrossRef](#)]
48. Parikh, A.; Madamwar, D. Partial Characterization of Extracellular Polysaccharides from Cyanobacteria. *Bioresour. Technol.* **2006**, *97*, 1822–1827. [[CrossRef](#)] [[PubMed](#)]
49. Paula, H.C.B.; Rodrigues, M.L.L.; Ribeiro, W.L.C.; Stadler, A.S.; Paula, R.C.M.; Abreu, F.O.M.S. Protective Effect of Cashew Gum Nanoparticles on Natural Larvicide from Moringa Oleifera Seeds. *J. Appl. Polym. Sci.* **2012**, *124*, 1778–1784. [[CrossRef](#)]
50. Ramesan, M.T.; Privya, P.P.; Jayakrishnan, P.; Kalaprasad, G.; Bahuleyan, B.K.; Al-Maghrabi, M.A. Influence of Magnetite Nanoparticles on Electrical, Magnetic and Thermal Properties of Chitin/Cashew Gum Biopolymer Nanocomposites. *Polym. Compos.* **2018**, *39*, E540–E549. [[CrossRef](#)]
51. Gholizadeh, A.; Shahrokhian, S.; Iraj Zad, A.; Mohajerzadeh, S.; Vosoughi, M.; Darbari, S.; Koohsorkhi, J.; Mehran, M. Fabrication of Sensitive Glutamate Biosensor Based on Vertically Aligned CNT Nanoelectrode Array and Investigating the Effect of CNTs Density on the Electrode Performance. *Anal. Chem.* **2012**, *84*, 5932–5938. [[CrossRef](#)] [[PubMed](#)]
52. Lux, F. Models Proposed to Explain the Electrical Conductivity of Mixtures Made of Conductive and Insulating Materials. *J. Mater. Sci.* **1993**, *28*, 285–301. [[CrossRef](#)]

Disclaimer/Publisher’s Note: The statements, opinions and data contained in all publications are solely those of the individual author(s) and contributor(s) and not of MDPI and/or the editor(s). MDPI and/or the editor(s) disclaim responsibility for any injury to people or property resulting from any ideas, methods, instructions or products referred to in the content.